EUROPEAN LABORATORY FOR PARTICLE PHYSICS

CERN-EP/98-197
December 10, 1998

Measurement of the W Mass and Width in e^+e^- Collisions at 183 GeV

The OPAL Collaboration

Abstract

Using a data sample of 57 pb^{-1} recorded at a centre-of-mass energy of 183 GeV with the OPAL detector at LEP, 282 $W^+W^- \to q\overline{q}q\overline{q}$ and 300 $W^+W^- \to q\overline{q}\ell\overline{\nu}_\ell$ candidate events are used to obtain a measurement of the mass of the W boson, $M_W = 80.39 \pm 0.13(\text{stat.}) \pm 0.05(\text{syst.})$ GeV, assuming the Standard Model relation between M_W and Γ_W. A second fit provides a direct measure of the width of the W boson and gives $\Gamma_W = 1.96 \pm 0.34(\text{stat.}) \pm 0.20(\text{syst.})$ GeV. These results are combined with previous OPAL results to obtain $M_W = 80.38 \pm 0.12(\text{stat.}) \pm 0.05(\text{syst.})$ GeV and $\Gamma_W = 1.84 \pm 0.32(\text{stat.}) \pm 0.20(\text{syst.})$ GeV.

(submitted to Physics Letters B)

The OPAL Collaboration

G. Abbiendi[2], K. Ackerstaff[8], G. Alexander[23], J. Allison[16], N. Altekamp[5], K.J. Anderson[9], S. Anderson[12], S. Arcelli[17], S. Asai[24], S.F. Ashby[1], D. Axen[29], G. Azuelos[18,a], A.H. Ball[17], E. Barberio[8], R.J. Barlow[16], R. Bartoldus[3], J.R. Batley[5], S. Baumann[3], J. Bechtluft[14], T. Behnke[27], K.W. Bell[20], G. Bella[23], A. Bellerive[9], S. Bentvelsen[8], S. Bethke[14], S. Betts[15], O. Biebel[14], A. Biguzzi[5], S.D. Bird[16], V. Blobel[27], I.J. Bloodworth[1], P. Bock[11], J. Böhme[14], D. Bonacorsi[2], M. Boutemeur[34], S. Braibant[8], P. Bright-Thomas[1], L. Brigliadori[2], R.M. Brown[20], H.J. Burckhart[8], P. Capiluppi[2], R.K. Carnegie[6], A.A. Carter[13], J.R. Carter[5], C.Y. Chang[17], D.G. Charlton[1,b], D. Chrisman[4], C. Ciocca[2], P.E.L. Clarke[15], E. Clay[15], I. Cohen[23], J.E. Conboy[15], O.C. Cooke[8], C. Couyoumtzelis[13], R.L. Coxe[9], M. Cuffiani[2], S. Dado[22], G.M. Dallavalle[2], R. Davis[30], S. De Jong[12], A. de Roeck[8], P. Dervan[15], K. Desch[8], B. Dienes[33,d], M.S. Dixit[7], J. Dubbert[34], E. Duchovni[26], G. Duckeck[34], I.P. Duerdoth[16], D. Eatough[16], P.G. Estabrooks[6], E. Etzion[23], F. Fabbri[2], M. Fanti[2], A.A. Faust[30], F. Fiedler[27], M. Fierro[2], I. Fleck[8], R. Folman[26], A. Fürtjes[8], D.I. Futyan[16], P. Gagnon[7], J.W. Gary[4], J. Gascon[18], S.M. Gascon-Shotkin[17], G. Gaycken[27], C. Geich-Gimbel[3], G. Giacomelli[2], P. Giacomelli[2], V. Gibson[5], W.R. Gibson[13], D.M. Gingrich[30,a], D. Glenzinski[9], J. Goldberg[22], W. Gorn[4], C. Grandi[2], K. Graham[28], E. Gross[26], J. Grunhaus[23], M. Gruwé[27], G.G. Hanson[12], M. Hansroul[8], M. Hapke[13], K. Harder[27], A. Harel[22], C.K. Hargrove[7], C. Hartmann[3], M. Hauschild[8], C.M. Hawkes[1], R. Hawkings[27], R.J. Hemingway[6], M. Herndon[17], G. Herten[10], R.D. Heuer[27], M.D. Hildreth[8], J.C. Hill[5], P.R. Hobson[25], M. Hoch[18], A. Hocker[9], K. Hoffman[8], R.J. Homer[1], A.K. Honma[28,a], D. Horváth[32,c], K.R. Hossain[30], R. Howard[29], P. Hüntemeyer[27], P. Igo-Kemenes[11], D.C. Imrie[25], K. Ishii[24], F.R. Jacob[20], A. Jawahery[17], H. Jeremie[18], M. Jimack[1], C.R. Jones[5], P. Jovanovic[1], T.R. Junk[6], D. Karlen[6], V. Kartvelishvili[16], K. Kawagoe[24], T. Kawamoto[24], P.I. Kayal[30], R.K. Keeler[28], R.G. Kellogg[17], B.W. Kennedy[20], D.H. Kim[19], A. Klier[26], S. Kluth[8], T. Kobayashi[24], M. Kobel[3,e], D.S. Koetke[6], T.P. Kokott[3], M. Kolrep[10], S. Komamiya[24], R.V. Kowalewski[28], T. Kress[4], P. Krieger[6], J. von Krogh[11], T. Kuhl[3], P. Kyberd[13], G.D. Lafferty[16], H. Landsman[22], D. Lanske[14], J. Lauber[15], S.R. Lautenschlager[31], I. Lawson[28], J.G. Layter[4], D. Lazic[22], A.M. Lee[31], D. Lellouch[26], J. Letts[12], L. Levinson[26], R. Liebisch[11], B. List[8], C. Littlewood[5], A.W. Lloyd[1], S.L. Lloyd[13], F.K. Loebinger[16], G.D. Long[28], M.J. Losty[7], J. Ludwig[10], D. Liu[12], A. Macchiolo[2], A. Macpherson[30], W. Mader[3], M. Mannelli[8], S. Marcellini[2], C. Markopoulos[13], A.J. Martin[13], J.P. Martin[18], G. Martinez[17], T. Mashimo[24], P. Mättig[26], W.J. McDonald[30], J. McKenna[29], E.A. Mckigney[15], T.J. McMahon[1], R.A. McPherson[28], F. Meijers[8], S. Menke[3], F.S. Merritt[9], H. Mes[7], J. Meyer[27], A. Michelini[2], S. Mihara[24], G. Mikenberg[26], D.J. Miller[15], R. Mir[26], W. Mohr[10], A. Montanari[2], T. Mori[24], K. Nagai[8], I. Nakamura[24], H.A. Neal[12], B. Nellen[3], R. Nisius[8], S.W. O'Neale[1], F.G. Oakham[7], F. Odorici[2], H.O. Ogren[12], M.J. Oreglia[9], S. Orito[24], J. Pálinkás[33,d], G. Pásztor[32], J.R. Pater[16], G.N. Patrick[20], J. Patt[10], R. Perez-Ochoa[8], S. Petzold[27], P. Pfeifenschneider[14], J.E. Pilcher[9], J. Pinfold[30], D.E. Plane[8], P. Poffenberger[28], J. Polok[8], M. Przybycień[8], C. Rembser[8], H. Rick[8], S. Robertson[28], S.A. Robins[22], N. Rodning[30], J.M. Roney[28], K. Roscoe[16], A.M. Rossi[2], Y. Rozen[22], K. Runge[10], O. Runolfsson[8], D.R. Rust[12], K. Sachs[10], T. Saeki[24], O. Sahr[34], W.M. Sang[25], E.K.G. Sarkisyan[23], C. Sbarra[29], A.D. Schaile[34], O. Schaile[34], F. Scharf[3], P. Scharff-Hansen[8], J. Schieck[11], B. Schmitt[8], S. Schmitt[11], A. Schöning[8], M. Schröder[8], M. Schumacher[3], C. Schwick[8], W.G. Scott[20], R. Seuster[14], T.G. Shears[8], B.C. Shen[4], C.H. Shepherd-Themistocleous[8], P. Sherwood[15], G.P. Siroli[2], A. Sittler[27], A. Skuja[17], A.M. Smith[8], G.A. Snow[17], R. Sobie[28], S. Söldner-Rembold[10], S. Spagnolo[20], M. Sproston[20], A. Stahl[3], K. Stephens[16], J. Steuerer[27], K. Stoll[10], D. Strom[19], R. Ströhmer[34], B. Surrow[8], S.D. Talbot[1], S. Tanaka[24], P. Taras[18], S. Tarem[22], R. Teuscher[8], M. Thiergen[10], J. Thomas[15], M.A. Thomson[8], E. von Törne[3], E. Torrence[8], S. Towers[6], I. Trigger[18], Z. Trócsányi[33], E. Tsur[23], A.S. Turcot[9], M.F. Turner-Watson[1], I. Ueda[24], R. Van Kooten[12], P. Vannerem[10], M. Verzocchi[10], H. Voss[3], F. Wäckerle[10], A. Wagner[27], C.P. Ward[5], D.R. Ward[5], P.M. Watkins[1], A.T. Watson[1], N.K. Watson[1], P.S. Wells[8], N. Wermes[3], J.S. White[6], G.W. Wilson[16], J.A. Wilson[1], T.R. Wyatt[16], S. Yamashita[24], G. Yekutieli[26], V. Zacek[18], D. Zer-Zion[8]

[1]School of Physics and Astronomy, University of Birmingham, Birmingham B15 2TT, UK
[2]Dipartimento di Fisica dell' Università di Bologna and INFN, I-40126 Bologna, Italy
[3]Physikalisches Institut, Universität Bonn, D-53115 Bonn, Germany
[4]Department of Physics, University of California, Riverside CA 92521, USA
[5]Cavendish Laboratory, Cambridge CB3 0HE, UK
[6]Ottawa-Carleton Institute for Physics, Department of Physics, Carleton University, Ottawa, Ontario K1S 5B6, Canada
[7]Centre for Research in Particle Physics, Carleton University, Ottawa, Ontario K1S 5B6, Canada
[8]CERN, European Organisation for Particle Physics, CH-1211 Geneva 23, Switzerland
[9]Enrico Fermi Institute and Department of Physics, University of Chicago, Chicago IL 60637, USA
[10]Fakultät für Physik, Albert Ludwigs Universität, D-79104 Freiburg, Germany
[11]Physikalisches Institut, Universität Heidelberg, D-69120 Heidelberg, Germany
[12]Indiana University, Department of Physics, Swain Hall West 117, Bloomington IN 47405, USA
[13]Queen Mary and Westfield College, University of London, London E1 4NS, UK
[14]Technische Hochschule Aachen, III Physikalisches Institut, Sommerfeldstrasse 26-28, D-52056 Aachen, Germany
[15]University College London, London WC1E 6BT, UK
[16]Department of Physics, Schuster Laboratory, The University, Manchester M13 9PL, UK
[17]Department of Physics, University of Maryland, College Park, MD 20742, USA
[18]Laboratoire de Physique Nucléaire, Université de Montréal, Montréal, Quebec H3C 3J7, Canada
[19]University of Oregon, Department of Physics, Eugene OR 97403, USA
[20]CLRC Rutherford Appleton Laboratory, Chilton, Didcot, Oxfordshire OX11 0QX, UK
[22]Department of Physics, Technion-Israel Institute of Technology, Haifa 32000, Israel
[23]Department of Physics and Astronomy, Tel Aviv University, Tel Aviv 69978, Israel
[24]International Centre for Elementary Particle Physics and Department of Physics, University of Tokyo, Tokyo 113-0033, and Kobe University, Kobe 657-8501, Japan
[25]Institute of Physical and Environmental Sciences, Brunel University, Uxbridge, Middlesex UB8 3PH, UK
[26]Particle Physics Department, Weizmann Institute of Science, Rehovot 76100, Israel
[27]Universität Hamburg/DESY, II Institut für Experimental Physik, Notkestrasse 85, D-22607 Hamburg, Germany
[28]University of Victoria, Department of Physics, P O Box 3055, Victoria BC V8W 3P6, Canada
[29]University of British Columbia, Department of Physics, Vancouver BC V6T 1Z1, Canada
[30]University of Alberta, Department of Physics, Edmonton AB T6G 2J1, Canada
[31]Duke University, Dept of Physics, Durham, NC 27708-0305, USA
[32]Research Institute for Particle and Nuclear Physics, H-1525 Budapest, P O Box 49, Hungary
[33]Institute of Nuclear Research, H-4001 Debrecen, P O Box 51, Hungary
[34]Ludwigs-Maximilians-Universität München, Sektion Physik, Am Coulombwall 1, D-85748 Garching, Germany

[a] and at TRIUMF, Vancouver, Canada V6T 2A3
[b] and Royal Society University Research Fellow
[c] and Institute of Nuclear Research, Debrecen, Hungary
[d] and Department of Experimental Physics, Lajos Kossuth University, Debrecen, Hungary
[e] on leave of absence from the University of Freiburg

1 Introduction

Comparison between direct measurements of the mass of the W boson, M_{W}, and the value determined indirectly from precise electroweak results from data taken at $\sqrt{s} \approx M_{\mathrm{Z}}$ and lower energies [1] provides an important test of the Standard Model. In addition, the direct measurement of M_{W} can be used to constrain the mass of the Higgs boson, M_{H}, by comparison with theoretical predictions involving radiative corrections sensitive to M_{H} [2]. The constraints imposed using M_{W}, which are presently limited by statistical uncertainties, are complementary to those imposed by other electroweak measurements, which are largely limited by theoretical uncertainties [3].

The first direct measurements of the W boson mass were performed at hadron colliders [4]. During 1996, the LEP collider at CERN began operating at centre-of-mass energies exceeding the $\mathrm{W^+W^-}$ production threshold (LEP2) thus allowing direct determinations of the mass of the W boson. The combination of direct measurements from LEP2 [5-9] and from hadron colliders presently yields $M_{\mathrm{W}} = 80.41 \pm 0.10$ GeV [10]. It is expected that LEP2 will ultimately achieve a precision on the W mass of approximately 30-40 MeV [11].

In 1997, OPAL collected 57 pb^{-1} of data at a centre-of-mass energy of approximately 183 GeV. This paper describes measurements of the W boson mass and width using this data sample.

2 The OPAL Detector

The OPAL detector includes a 3.7 m diameter tracking volume immersed in a 0.435 T axial magnetic field, which yields a transverse[1] momentum resolution of $\sigma_{p_{xy}}/p_{xy} \approx \sqrt{(0.020)^2 + (0.0015 \cdot p_{xy})^2/\mathrm{GeV}^2}$ and an average angular resolution of about 0.3 mrad in ϕ and 1 mrad in θ. The electromagnetic calorimeter consists of 11 704 lead glass blocks with full azimuthal acceptance in the range $|\cos\theta| < 0.98$ and a relative energy resolution of approximately 3% at $E \approx 47$ GeV, the mean energy of electrons from W decays. The magnet return yoke is instrumented with streamer tubes to serve as the hadronic calorimeter. Muon chambers surrounding the hadronic calorimeter provide muon identification over the range $|\cos\theta| < 0.98$. Jets are constructed from charged tracks and energy deposits in the electromagnetic and hadronic calorimeters using the Durham algorithm [12]. The energies of reconstructed jets are calculated using the technique described in [13]. Using $\mathrm{e^+e^-} \to \mathrm{q\overline{q}}$ data taken at $\sqrt{s} = 91$ GeV, the jet energy resolution is determined to be approximately $\sigma_E/E \approx 20\%$ with an angular resolution of 20-30 mrad depending on the jet visible energy and polar angle. A more detailed description of the OPAL detector can be found in [14].

3 Data and Monte Carlo Samples

The integrated luminosity of the data sample, evaluated using small angle Bhabha scattering events observed in the silicon tungsten forward calorimeter, is $57.21 \pm 0.15(\mathrm{stat.}) \pm 0.20(\mathrm{syst.})$ pb^{-1}. The mean centre-of-mass energy, weighted by luminosity, is $\sqrt{s} = 182.68 \pm 0.05$ GeV [15].

[1] The OPAL coordinate system is defined such that the z-axis is parallel to and in the direction of the $\mathrm{e^-}$ beam, the x-axis lies in the plane of the accelerator pointing towards the centre of the LEP ring, and the y-axis is normal to the plane of the accelerator and has its positive direction defined to yield a right-handed coordinate system. The azimuthal angle, ϕ, and the polar angle, θ, are the conventional spherical coordinates.

3.1 Event Selections

The event selections are described in detail in [16]. The selections are sensitive to the leptonic $\mathrm{W^+W^-} \to \ell^+\nu_\ell\ell'^-\overline{\nu}_{\ell'}$, semi-leptonic $\mathrm{W^+W^-} \to \mathrm{q\overline{q}}\ell\overline{\nu}_\ell$ and hadronic $\mathrm{W^+W^-} \to \mathrm{q\overline{q}q\overline{q}}$ final states. By construction, the selections are mutually exclusive. The leptonic final state is not used in this analysis.

Semi-leptonic $\mathrm{W^+W^-} \to \mathrm{q\overline{q}}\ell\overline{\nu}_\ell$ decays comprise 44% of the total $\mathrm{W^+W^-}$ cross-section. The selection employs three multivariate relative likelihood discriminants, one for each of the $\mathrm{W^+W^-} \to \mathrm{q\overline{q}e\overline{\nu}_e}$, $\mathrm{W^+W^-} \to \mathrm{q\overline{q}}\mu\overline{\nu}_\mu$ and $\mathrm{W^+W^-} \to \mathrm{q\overline{q}}\tau\overline{\nu}_\tau$ final states. The $\mathrm{W^+W^-} \to \mathrm{q\overline{q}e\overline{\nu}_e}$ and $\mathrm{W^+W^-} \to \mathrm{q\overline{q}}\mu\overline{\nu}_\mu$ channels are characterized by two well-separated hadronic jets, a high-momentum lepton and missing momentum due to the prompt neutrino from the leptonic W decay. The $\mathrm{W^+W^-} \to \mathrm{q\overline{q}}\tau\overline{\nu}_\tau$ channel is characterized similarly except that the τ lepton is identified as an isolated, low-multiplicity jet typically consisting of one or three charged tracks. After all cuts, $\mathrm{W^+W^-} \to \mathrm{q\overline{q}}\ell\overline{\nu}_\ell$ events are selected with an efficiency of 85% and a purity of 90%. The dominant backgrounds are $\mathrm{Z^0}/\gamma \to \mathrm{q\overline{q}}$ and four-fermion processes such as $\mathrm{e^+e^-} \to \mathrm{We\overline{\nu}_e}$ and $(\mathrm{Z^0}/\gamma)^*(\mathrm{Z^0}/\gamma)^* \to \mathrm{q\overline{q}}\ell^+\ell^-$.

Hadronic $\mathrm{W^+W^-} \to \mathrm{q\overline{q}q\overline{q}}$ decays comprise 46% of the total $\mathrm{W^+W^-}$ cross-section and are characterized by four energetic hadronic jets and little or no missing energy. A loose preselection removes approximately 98% of the dominant background process, $\mathrm{Z^0}/\gamma \to \mathrm{q\overline{q}}$. Following the preselection, a multivariate relative likelihood discriminant is employed to select the $\mathrm{W^+W^-} \to \mathrm{q\overline{q}q\overline{q}}$ candidates with an efficiency of 85% and a purity of 78%.

After these selections, 361 $\mathrm{W^+W^-} \to \mathrm{q\overline{q}}\ell\overline{\nu}_\ell$ and 438 $\mathrm{W^+W^-} \to \mathrm{q\overline{q}q\overline{q}}$ candidate events are identified, consistent with Standard Model expectations [16]. As discussed in Section 4.1, additional cuts are applied to remove poorly reconstructed events and further reduce backgrounds.

3.2 Monte Carlo Samples

A number of Monte Carlo simulation programs are used to provide estimates of efficiencies and purities as well as the shapes of the W mass distributions. The majority of the samples are generated at $\sqrt{s} =$ 183 GeV assuming $M_\mathrm{W} = 80.33$ GeV. All Monte Carlo samples include a full simulation of the OPAL detector [17].

The main $\mathrm{W^+W^-}$ samples are generated using KORALW [18] and include only the CC03 diagrams[2]. The four-fermion backgrounds $\mathrm{We\overline{\nu}_e}$ and $(\mathrm{Z^0}/\gamma)^*(\mathrm{Z^0}/\gamma)^*$ are simulated using PYTHIA [19], while grc4f [20] and EXCALIBUR [21] are used to estimate systematic uncertainties. The background process $\mathrm{Z^0}/\gamma \to \mathrm{q\overline{q}}$ is simulated using PYTHIA, with HERWIG [22] used as an alternative to assess possible systematic effects.

4 Measurement of the Mass and Width of the W Boson

The W boson mass, M_W, and decay width, Γ_W, are determined from fits to the reconstructed invariant mass spectrum of the selected $\mathrm{W^+W^-} \to \mathrm{q\overline{q}}\ell\overline{\nu}_\ell$ and $\mathrm{W^+W^-} \to \mathrm{q\overline{q}q\overline{q}}$ events. For each selected event, a kinematic fit is employed to improve the mass resolution and further reduce background. A reweighting

[2] In this paper, the doubly-resonant W pair production diagrams, *i.e.* t-channel ν_e exchange and s-channel $\mathrm{Z^0}/\gamma$ exchange, are referred to as "CC03", following the notation of [11].

technique [11] is used to produce Monte Carlo mass spectra corresponding to any given mass and width. A binned likelihood fit is used to determine M_{W} and Γ_{W} by comparing the shape of the reconstructed invariant mass distribution from the data to that from reweighted Monte Carlo spectra.

Two alternative methods are also used to extract M_{W}. In the first, an analytic fit to the measured mass spectrum uses an unbinned likelihood fit to determine M_{W}. To describe the signal shape, the fit uses a parametrization based on a Breit-Wigner function [5]. The second method uses a convolution technique similar to that used by the DELPHI Collaboration [6]. These alternative fits have sensitivities similar to that of the reweighting fit and are used as cross-checks.

4.1 Invariant Mass Reconstruction

The three methods for extracting M_{W} use essentially the same procedures to reconstruct the invariant mass of the W candidates. The description provided here applies to the reweighting method. Small variations relevant for the alternative analyses are discussed in Section 4.3.

For the selected $\mathrm{W^+W^-} \to \mathrm{q\overline{q}q\overline{q}}$ events tracks and clusters are grouped into four jets using the Durham algorithm. A kinematic fit is then performed to estimate the reconstructed invariant mass of the W candidate. The fit incorporates the constraints of energy and momentum conservation (4C fit) yielding two reconstructed masses per event, one for each W boson in the final state. An additional constraint can be incorporated by neglecting the finite W width and constraining the masses of the two W boson candidates to be equal (5C fit), thus yielding a single reconstructed invariant mass for each event. The kinematic fit employs the method of Lagrange multipliers and a χ^2-minimization technique. For extracting M_{W} from the $\mathrm{W^+W^-} \to \mathrm{q\overline{q}q\overline{q}}$ candidates, the 5C fit is used to determine a reconstructed invariant mass, m_{rec}, its error, σ_{rec}, and a χ^2 fit-probability for each event. The measured jet momenta with their associated errors and the measured jet masses are used as inputs. The use of the measured jet masses, rather than treating the jets as massless, improves the fitted mass resolution. Based on Monte Carlo studies, the errors associated with the measured jet momentum are parameterized as functions of the visible energy and polar angle of the jet.

For each $\mathrm{W^+W^-} \to \mathrm{q\overline{q}q\overline{q}}$ event three kinematic fits are performed, corresponding to the three possible jet pairings. This ambiguity in the choice of the jet pairing leads to a combinatorial background. To eliminate poorly reconstructed events and reduce backgrounds, only combinations which yield a 5C fit with a χ^2 fit-probability exceeding 0.01 and $m_{\mathrm{rec}} > 65$ GeV are considered. In addition, combinations with $\sigma_{\mathrm{rec}} < 0.5$ GeV are excluded[3]. A relative likelihood discriminant is employed to choose a single combination for each event. The likelihood is constructed for each surviving combination and takes as input the following three variables: the difference between the two fitted masses resulting from a 4C fit, the sum of the di-jet opening angles and the 5C fit mass. The resulting jet-pairing likelihood distribution is shown in Figure 1. For each event, the combination corresponding to the largest jet-pairing likelihood is retained provided it has a likelihood output exceeding 0.18. If the combination fails to satisfy this criterion, the event is not used. The cut of 0.18 on the jet-pairing likelihood is chosen to optimize the product of efficiency and purity. Approximately 69% of selected $\mathrm{W^+W^-} \to \mathrm{q\overline{q}q\overline{q}}$ events survive, while 60% of the background is removed. Most of the rejected events fail the cut on the χ^2 fit-probability. Monte Carlo studies estimate that in 87% of the surviving signal events, the selected combination corresponds to the correct jet pairing and that this fraction is independent of M_{W} to within 0.1% over a ± 1 GeV range. The number of surviving events in the $\mathrm{W^+W^-} \to \mathrm{q\overline{q}q\overline{q}}$ channel is given in Table 1.

[3]Fits which yield $\sigma_{\mathrm{rec}} < 0.5$ GeV are excluded because Monte Carlo studies reveal that the reconstructed mass resolution of these events is very poor; these events often have a reconstructed invariant mass close to the kinematic limit and are assigned an anomalously small fit error.

In the selected $W^+W^- \to q\overline{q}e\overline{\nu}_e$ and $W^+W^- \to q\overline{q}\mu\overline{\nu}_\mu$ events the non-leptonic part of the event is reconstructed as two jets using the Durham algorithm. A kinematic fit is then performed incorporating the same five constraints as employed for the $W^+W^- \to q\overline{q}q\overline{q}$ events. This results in a 2C fit since the three-momentum of the neutrino is not known. For the leptons, the inputs to the kinematic fit are the lepton energy and direction and their associated errors. The direction is estimated using the track associated with the electron or muon candidate. The energy is estimated from the associated electromagnetic calorimeter cluster for electrons and from the momentum of the associated track for muons. Jets are treated in the manner described above. Only events with a χ^2 fit-probability exceeding 0.001, $m_{\rm rec} > 65$ GeV and $\sigma_{\rm rec} > 0.5$ GeV are retained. These cuts reduce backgrounds by roughly 55% and remove poorly reconstructed events. Since the $W^+W^- \to q\overline{q}\ell\overline{\nu}_\ell$ event selections already yield low backgrounds, the cut on the χ^2 fit-probability is looser than for the $W^+W^- \to q\overline{q}q\overline{q}$ channel. Approximately 90% and 92% of selected $W^+W^- \to q\overline{q}e\overline{\nu}_e$ and $W^+W^- \to q\overline{q}\mu\overline{\nu}_\mu$ events, respectively, satisfy these additional criteria. Most of the rejected events fail the cut on the χ^2 fit-probability. The numbers of surviving events are listed in Table 1.

The Selected $W^+W^- \to q\overline{q}\tau\overline{\nu}_\tau$ events are also reconstructed as two jets using the Durham algorithm after excluding the tracks and clusters associated with the tau. The invariant mass of the jet-jet system, scaled by the ratio of the beam energy to the sum of the jet energies, and its associated error are used in determining $M_{\rm W}$ from this channel. Only events with a reconstructed invariant mass greater than 65 GeV and an error on the reconstructed invariant mass greater than 0.5 GeV are retained. In addition, to further reduce background, a 1C fit is performed and the resulting χ^2 fit-probability is required to exceed 0.001. The fit incorporates the same five constraints as employed for the $W^+W^- \to q\overline{q}q\overline{q}$ channel, assumes that the τ lepton direction is given by the direction of the visible decay products associated with the tau and estimates the total energy of the tau using energy and momentum constraints. Approximately 78% of selected $W^+W^- \to q\overline{q}\tau\overline{\nu}_\tau$ events satisfy these additional criteria while 65% of the background is removed. Most of the rejected events fail the cut on the χ^2 fit-probability. The number of surviving events is listed in Table 1.

The full width at half maximum of the residual of the reconstructed invariant mass per event is used as an estimate of the average $m_{\rm rec}$ resolution and is calculated using Monte Carlo events in which less than 100 MeV of energy is radiated into initial state photons. For $W^+W^- \to q\overline{q}q\overline{q}$ events this resolution is 1.7 GeV for fits corresponding to the correct jet pairing. For $W^+W^- \to q\overline{q}\ell\overline{\nu}_\ell$ events the average $m_{\rm rec}$ resolution per event is 2.4, 2.8 and 3.4 GeV in the $W^+W^- \to q\overline{q}e\overline{\nu}_e$, $W^+W^- \to q\overline{q}\mu\overline{\nu}_\mu$ and $W^+W^- \to q\overline{q}\tau\overline{\nu}_\tau$ channels, respectively.

4.2 Extraction of the W Mass and Width

The W boson mass and width are extracted by directly comparing the reconstructed mass distribution of the data to mass spectra obtained from fully simulated Monte Carlo events corresponding to various values of $M_{\rm W}$ and $\Gamma_{\rm W}$. A likelihood fit is used to extract $M_{\rm W}$ and $\Gamma_{\rm W}$ by determining which Monte Carlo spectrum best describes the data. The Monte Carlo spectra for arbitrary values of $M_{\rm W}$ and $\Gamma_{\rm W}$ are obtained using the Monte Carlo reweighting technique described in [5].

The mass spectra for background events are taken from Monte Carlo and are assumed to be independent of $M_{\rm W}$ and $\Gamma_{\rm W}$. The background reconstructed mass distributions are normalised to the expected number of background events. The reweighted signal spectra are then normalised such that the total number of signal plus background events corresponds to the observed number of events. This is done separately for the $W^+W^- \to q\overline{q}q\overline{q}$, $W^+W^- \to q\overline{q}e\overline{\nu}_e$, $W^+W^- \to q\overline{q}\mu\overline{\nu}_\mu$ and $W^+W^- \to q\overline{q}\tau\overline{\nu}_\tau$ channels. In addition, the $W^+W^- \to q\overline{q}\ell\overline{\nu}_\ell$ channels are divided into four subsamples according to the error on the reconstructed invariant mass. These subsamples are treated independently within each

channel. This division gives a larger weight to events with reconstructed masses which are known with better precision (*i.e.* small $\sigma_{\rm rec}$) relative to events with poorly determined $m_{\rm rec}$ and reduces the expected statistical uncertainty on the fitted W mass by approximately 7% in the $\mathrm{W^+W^-} \to \mathrm{q\overline{q}}\ell\overline{\nu}_\ell$ channels. In the $\mathrm{W^+W^-} \to \mathrm{q\overline{q}q\overline{q}}$ channel, the width of the reconstructed mass distribution is dominated by the intrinsic width of the W so that a similar subdivision does not improve the $M_{\rm W}$ sensitivity in this channel and therefore is not implemented. The $\sigma_{\rm rec}$ distribution is shown in Figure 2 for the $\mathrm{W^+W^-} \to \mathrm{q\overline{q}q\overline{q}}$ and $\mathrm{W^+W^-} \to \mathrm{q\overline{q}}\ell\overline{\nu}_\ell$ channels separately.

A binned log-likelihood fit to the $m_{\rm rec}$ distributions of the data is performed in the range $m_{\rm rec} > 65$ GeV. The log-likelihood function is defined as

$$\ln(\mathcal{L}) = \sum_{i=1}^{N_{\rm bins}} n_i \ln\left(f_b\,\mathcal{P}_b^i + (1-f_b)\,\mathcal{P}_s^i(M_{\rm W},\Gamma_{\rm W})\right),$$

where n_i is the number of observed events in the ith bin, f_b is the expected background fraction of the sample using the normalization procedure described above, $\mathcal{P}_s^i(M_{\rm W},\Gamma_{\rm W})$ is the probability of observing a signal event in the ith bin assuming a W boson mass and width of $M_{\rm W}$ and $\Gamma_{\rm W}$ and $\mathcal{P}_b^i$ is the analogous probability for the background, which is assumed to be independent of the W mass and width. Both $\mathcal{P}_s^i(M_{\rm W},\Gamma_{\rm W})$ and $\mathcal{P}_b^i$ are estimated using the relevant Monte Carlo spectrum. The log-likelihood curve is determined separately for each channel. For the $\mathrm{W^+W^-} \to \mathrm{q\overline{q}}\ell\overline{\nu}_\ell$ channels, the results are obtained by adding the log-likelihood curves separately determined from each subsample.

Two types of fit are performed. In the one-parameter fit, $\Gamma_{\rm W}$ is constrained to its Standard Model relation to the W mass [5] and only $M_{\rm W}$ is determined. The results of this fit for each channel are given in Table 2 and displayed in Figure 3. The combined result is discussed in Section 6. In the two-parameter fit, both $M_{\rm W}$ and $\Gamma_{\rm W}$ are determined simultaneously. The likelihood contours for this fit are displayed in Figure 4 including statistical errors only. The systematic uncertainties are discussed in Section 5.

One advantage of the reweighting method is that the fitted parameters should be unbiased since any offsets introduced in the analysis are implicitly accounted for in the Monte Carlo spectra used in the reweighting procedure. This is verified using several Monte Carlo samples generated at various $M_{\rm W}$ and $\Gamma_{\rm W}$. In addition, tests using a large ensemble of Monte Carlo subsamples, each corresponding to 57 pb^{-1} and including background contributions, are used to verify for each channel separately and for all channels combined, that the measured fit errors accurately reflect the RMS spread of the residual distribution for both the $M_{\rm W}$ and $\Gamma_{\rm W}$ fits.

4.3 Alternative Fit Methods

4.3.1 Breit-Wigner Fit

The Breit-Wigner method is analogous to that described in [5]. It employs an unbinned maximum-likelihood fit to the reconstructed mass spectrum using an analytic Breit-Wigner function to describe the signal. Due to initial-state radiation, the reconstructed mass spectrum is significantly asymmetric for data taken at $\sqrt{s} \approx 183$ GeV. It is found that a relativistic Breit-Wigner function, with different widths above and below the peak, gives a satisfactory description of the $m_{\rm rec}$ lineshape. The function is given by

$$S(m_{\rm rec}) = A\frac{m_{\rm rec}^2\,\Gamma_{-/+}^2}{(m_{\rm rec}^2 - m_0^2)^2 + m_{\rm rec}^2\,\Gamma_{-/+}^2},$$

where $\Gamma_{+(-)}$ is the width assumed for all $m_{\rm rec}$ above (below) the peak, m_0. The widths are fixed to values determined from fits to $\mathrm{W^+W^-}$ signal Monte Carlo samples and are found to be independent of $M_{\rm W}$ over the range relevant for this analysis. The shapes of the background distributions and the background fraction are also determined from Monte Carlo. The background fraction is held constant in the fit. The fit is performed over the range $70 < m_{\rm rec} < 88$ GeV.

For the $\mathrm{W^+W^-} \to \mathrm{q\overline{q}q\overline{q}}$ events, the likelihood method for choosing which jet pairing to use is found to distort the $m_{\rm rec}$ distribution so that it is inadequately described by a Breit-Wigner function. Therefore, the following procedure is employed [5]. The reconstructed invariant mass of the combination with the largest fit probability, P_1, is used if $P_1 > 0.01$. The reconstructed invariant mass of the combination with the second largest fit probability, P_2, is also used if it satisfies $P_2 > 0.01$ and $P_2 > P_1/3$. The selected reconstructed masses enter the same distribution with unit weight. Monte Carlo studies estimate that the correct combination is among those chosen in 90% of the surviving $\mathrm{W^+W^-} \to \mathrm{q\overline{q}q\overline{q}}$ events.

In contrast to the procedure employed for the reweighting method, the $\mathrm{W^+W^-} \to \mathrm{q\overline{q}}\ell\overline{\nu}_\ell$ events are not divided into subsamples according to $\sigma_{\rm rec}$ because the subsamples exhibit a distorted reconstructed mass distribution which is poorly described by a Breit-Wigner function.

The fitted mass, m_0, must be corrected for offsets not accounted for in the fit, *e.g.* from initial-state radiation and event selection. A correction is determined using fully simulated Monte Carlo samples generated at various known $M_{\rm W}$ and $\sqrt{s}$ with the expected background contributions included and is found to depend linearly on both $M_{\rm W}$ and $\sqrt{s}$. The results from the $\mathrm{W^+W^-} \to \mathrm{q\overline{q}q\overline{q}}$ and $\mathrm{W^+W^-} \to \mathrm{q\overline{q}}\ell\overline{\nu}_\ell$ channels, after correction, are given in Table 3.

4.3.2 Convolution Fit

The convolution method is similar to that employed by the DELPHI Collaboration [6]. The method attempts to exploit all available information by constructing a likelihood curve for each selected event. The likelihood is calculated using the functional expression

$$\mathcal{L}(M_{\rm W}, m_{\rm rec}) = p_s \mathcal{P}_s(M_{\rm W}, m_{\rm rec}),$$

where p_s is the probability of the candidate event being a real signal event and $\mathcal{P}_s$ is the probability density function for the signal,

$$\mathcal{P}_s(M_{\rm W}, m_{\rm rec}) = \mathrm{BW}(M_{\rm W}, m) \otimes \mathrm{R}(m, m_{\rm rec}),$$

where $\mathrm{R}(m, m_{\rm rec})$ is the resolution function estimated from the Monte Carlo and $\mathrm{BW}(M_{\rm W}, m)$ is a relativistic Breit-Wigner function with $\Gamma_{\rm W}$ fixed to its Standard Model relation to $M_{\rm W}$. The exact expression for the likelihood is channel dependent. For example, in the $\mathrm{W^+W^-} \to \mathrm{q\overline{q}q\overline{q}}$ channel the added complication of combinatorial background requires a sum over the three jet pairings. The log-likelihood curves from each selected event are summed to yield a single curve from which a fitted mass is determined. This fitted mass is corrected for background effects and for offsets not accounted for in the fit in the manner described for the Breit-Wigner fit. The results from the $\mathrm{W^+W^-} \to \mathrm{q\overline{q}q\overline{q}}$ and $\mathrm{W^+W^-} \to \mathrm{q\overline{q}}\ell\overline{\nu}_\ell$ channels, after all corrections, are given in Table 3.

5 Systematic Uncertainties

The systematic uncertainties are estimated as described below and summarised in Table 4.

Beam Energy:

The average LEP beam energy is known to a precision of ± 25 MeV [15]. The effect of this uncertainty on the measured M_{W} is determined from fits to large Monte Carlo samples for which the analysis is repeated assuming $\sqrt{s} = E_{\mathrm{cm}}^{\mathrm{MC}} \pm 50$ MeV. The observed shifts in the fitted M_{W} are used to estimate the associated systematic uncertainty. The spread in LEP beam energy of 152 ± 8 MeV [15] has a negligible effect on both the mass and width determinations.

Initial State Radiation:

The systematic error associated with uncertainties in the modelling of initial state radiation is estimated by comparing fully simulated KORALW Monte Carlo $\mathrm{W^+W^-}$ events generated using a leading logarithm $O(\alpha)$ treatment of initial state radiation to the standard $\mathrm{W^+W^-}$ sample which includes a next-to-leading-log $O(\alpha^2)$ treatment. No significant difference is observed and the statistical uncertainty of the comparison is taken as the associated systematic error.

Hadronization:

The scale of hadronization effects is studied by comparing the fit results of a single $\mathrm{W^+W^-}$ sample generated once using PYTHIA and again using HERWIG as the hadronization model. Both samples contain the same $\mathrm{W^+W^-}$ final states and differ only in their hadronization modelling. No significant differences are observed and the statistical uncertainty of the comparison is taken as the associated systematic error. As a cross-check, $\mathrm{W^+W^-}$ samples are generated with variations of the JETSET fragmentation parameters σ_q, b, Λ_{QCD} and Q_0, of one standard deviation about their tuned values [23]. The fit results are compared and yield no statistically significant effects.

Four-fermion Effects:

The Monte Carlo samples used to estimate background contributions in the reweighting procedure do not include a complete set of four-fermion diagrams and neglect interference effects between $\mathrm{W^+W^-}$ diagrams and other four-fermion processes. In order to test the sensitivity of the results to these effects, the fit results of a sample generated including the full set of interfering four-fermion diagrams are compared to those of a sample restricted to the CC03 $\mathrm{W^+W^-}$ diagrams alone. The comparison is performed using both the grc4f and the EXCALIBUR generators. In neither case is a significant difference observed. The larger of the two statistical uncertainties is assigned as the associated systematic error.

Detector Effects:

The effects of detector mis-calibrations and deficiencies in the Monte Carlo simulation of the data are investigated by varying the jet and lepton energy scales and the errors input to the kinematic fit over reasonable ranges. The ranges are dependent on polar angle and are determined from detailed comparisons between 1997 data and Monte Carlo using approximately $2.1\,\mathrm{pb}^{-1}$ of data collected at $\sqrt{s} \approx M_{\mathrm{Z}}$ and $\mathrm{e^+e^-} \to \mathrm{e^+e^-}$ events recorded at $\sqrt{s} \approx 183$ GeV. Of particular importance for the $\mathrm{W^+W^-} \to \mathrm{q\overline{q}}\ell\overline{\nu}_\ell$ channel are the lepton energy scales, which are varied by $\pm 0.5\%$. For the $\mathrm{W^+W^-} \to \mathrm{q\overline{q}q\overline{q}}$ channels the most important variations are for the errors associated with the jet angles, which are varied by $\pm 7\%$ for errors in $\cos\theta$ and $\pm 3\%$ for errors in ϕ. The jet energy scale is varied by ± 1–2% over most of $|\cos\theta|$. For each variation a large Monte Carlo sample is refitted and the resulting shifts in the fitted M_{W} are added in quadrature to yield an estimate of the associated systematic error.

Fit Procedure:

The reweighting procedure accounts for the fact that the Monte Carlo samples are generated at a centre-of-mass energy different from that of the data [5]. Monte Carlo samples generated at $\sqrt{s} = 182$ and 184 GeV are used to test this procedure and assign a systematic error.

The three methods used to measure M_{W} each utilise the data and Monte Carlo in different ways. A comparison of the fitted results is used to test for residual biases in the reweighting

fit. The three methods are compared using an ensemble of Monte Carlo subsamples, each corresponding to 57 pb^{-1} and including background. For each subsample the difference in the fitted M_{W} determined using the reweighting method and that determined using each of the other methods is calculated for the $\mathrm{W^+W^-} \to \mathrm{q\overline{q}q\overline{q}}$ and $\mathrm{W^+W^-} \to \mathrm{q\overline{q}}\ell\overline{\nu}_\ell$ channels separately and for the combined sample. The distributions of these differences are approximately Gaussian and have means consistent with zero and RMS values of approximately 90 MeV, 95 MeV, and 75 MeV (100 MeV, 75 MeV, and 60 MeV) when comparing the reweighting fits to the Breit-Wigner (convolution) fits in the $\mathrm{W^+W^-} \to \mathrm{q\overline{q}q\overline{q}}$, $\mathrm{W^+W^-} \to \mathrm{q\overline{q}}\ell\overline{\nu}_\ell$ and the combined samples, respectively. Since these alternative analyses yield results consistent with those obtained using the default reweighting analysis, no additional systematic is assigned based on these comparisons.

Background Treatment:

Uncertainties associated with both the normalization and shape of the background distributions are investigated. The background normalization is varied by one standard deviation of its associated uncertainties as evaluated in [16] and the data are refitted. As an estimate of the errors associated with the uncertainties in the shape of the background distributions, a variety of substitutions are made. For all channels, HERWIG replaced PYTHIA for the hadronization model for the $\mathrm{Z}^0/\gamma \to \mathrm{q\overline{q}}$ background. In addition, for the $\mathrm{W^+W^-} \to \mathrm{q\overline{q}q\overline{q}}$ channel, data taken at $\sqrt{s} \approx M_{\mathrm{Z}}$, scaled by $(183\,\mathrm{GeV}/M_{\mathrm{Z}})$, are also substituted for the $\mathrm{Z}^0/\gamma \to \mathrm{q\overline{q}}$ background. For each substitution the data are refitted. The quadrature sum of the shift in fitted mass observed when changing the normalization and the largest of the observed shifts in the fitted mass from the various substitutions in each channel is assigned as a systematic error. Using PYTHIA samples of $\mathrm{e^+e^-} \to \mathrm{We\overline{\nu}_e}$ events generated using various M_{W}, it is verified that the uncertainty on M_{W} has a negligible effect on the background distributions.

Monte Carlo Statistics:

The finite statistics of the Monte Carlo samples used in the reweighting procedure contribute a systematic uncertainty of ± 15 MeV to the W mass determined separately in the $\mathrm{W^+W^-} \to \mathrm{q\overline{q}q\overline{q}}$ and $\mathrm{W^+W^-} \to \mathrm{q\overline{q}}\ell\overline{\nu}_\ell$ channels, and ± 40 MeV to the W width determined from the combined sample.

Colour-Reconnection Effects and Bose-Einstein Correlations:

As discussed in [11] and [24] and references therein, a significant bias to the apparent W mass measured in the $\mathrm{W^+W^-} \to \mathrm{q\overline{q}q\overline{q}}$ channel could arise from the effects of colour-reconnection and/or Bose-Einstein correlations between the decay products of the $\mathrm{W^+}$ and $\mathrm{W^-}$. These effects are investigated separately.

Using currently available $\mathrm{W^+W^-}$ data, it is not possible to discern whether or not Bose-Einstein correlations are present between hadrons originating from different W decays [25-26]. To investigate possible systematic biases a Monte Carlo sample is generated including Bose-Einstein correlations using the PYTHIA Monte Carlo generator implemented as described in [27]. The fit result in the $\mathrm{W^+W^-} \to \mathrm{q\overline{q}q\overline{q}}$ channel from this sample is compared to a fit from a PYTHIA sample which excludes Bose-Einstein correlations. No significant bias is observed for the fitted parameters and the statistical precision of the comparison is taken as the associated systematic error of ± 32 MeV in the fitted mass determined from the $\mathrm{W^+W^-} \to \mathrm{q\overline{q}q\overline{q}}$ channel. The uncertainty on the fitted width in $\mathrm{W^+W^-} \to \mathrm{q\overline{q}q\overline{q}}$ channel propagates to an uncertainty of ± 55 MeV on the fitted width determined from the combined sample.

To investigate the systematic biases originating from colour-reconnection effects, several models are studied using the PYTHIA and ARIADNE [28] Monte Carlo generators. As discussed in the accompanying paper [29], comparing various event shapes offers a means of discriminating between the models and, when comparing with data, a means of testing each model independently of the M_{W} measurement. Based on these studies, and comparing fitted masses between Monte

Carlo samples including and excluding colour-reconnection effects, a systematic uncertainty of ± 49 MeV is assigned to the mass determined from the $\mathrm{W^+W^-} \to \mathrm{q\overline{q}q\overline{q}}$ channel [29]. The uncertainty on the fitted width in $\mathrm{W^+W^-} \to \mathrm{q\overline{q}q\overline{q}}$ channel propagates to an uncertainty of ± 109 MeV on the fitted width determined from the combined sample.

The contributions from each of the above sources are added in quadrature to yield the total systematic uncertainty. For the alternative analyses, the systematics are estimated similarly and yield comparable results.

6 Results

For the reweighting method described in Section 4.2, the results of a simultaneous fit to M_{W} and Γ_{W} from the combined $\mathrm{W^+W^-} \to \mathrm{q\overline{q}q\overline{q}}$ and $\mathrm{W^+W^-} \to \mathrm{q\overline{q}}\ell\overline{\nu}_\ell$ event samples are

$$\begin{aligned} M_{\mathrm{W}} &= 80.39 \pm 0.13 \pm 0.06 \text{ GeV}, \\ \Gamma_{\mathrm{W}} &= 1.96 \pm 0.34 \pm 0.20 \text{ GeV}, \end{aligned}$$

where the uncertainties are statistical and systematic, respectively. The correlation coefficient between M_{W} and Γ_{W} is 0.13. For this fit, the central values are determined by adding the log-likelihood curves from the $\mathrm{W^+W^-} \to \mathrm{q\overline{q}q\overline{q}}$ and $\mathrm{W^+W^-} \to \mathrm{q\overline{q}}\ell\overline{\nu}_\ell$ channels. The systematic uncertainties are also estimated by summing the log-likelihood curves from each channel.

A one-parameter fit for the mass is performed by constraining the width using the Standard Model relation to give $M_{\mathrm{W}} = 80.53 \pm 0.23(\mathrm{stat}) \pm 0.09(\mathrm{syst})$ GeV in the $\mathrm{W^+W^-} \to \mathrm{q\overline{q}q\overline{q}}$ channel, and $M_{\mathrm{W}} = 80.33 \pm 0.17(\mathrm{stat}) \pm 0.06(\mathrm{syst})$ GeV in the $\mathrm{W^+W^-} \to \mathrm{q\overline{q}}\ell\overline{\nu}_\ell$ channel. The combined result is determined taking into account the correlated systematics between the $\mathrm{W^+W^-} \to \mathrm{q\overline{q}q\overline{q}}$ and $\mathrm{W^+W^-} \to \mathrm{q\overline{q}}\ell\overline{\nu}_\ell$ channels and gives

$$M_{\mathrm{W}} = 80.39 \pm 0.13 \pm 0.05 \text{ GeV},$$

where the uncertainties are statistical and systematic, respectively. For the combination, the $\mathrm{W^+W^-} \to \mathrm{q\overline{q}q\overline{q}}$ channel carries a weight of 0.34. The combined $\mathrm{W^+W^-} \to \mathrm{q\overline{q}q\overline{q}}$ and $\mathrm{W^+W^-} \to \mathrm{q\overline{q}}\ell\overline{\nu}_\ell$ results from the alternative analyses, after all corrections, are for the Breit-Wigner fit, $M_{\mathrm{W}} = 80.37 \pm 0.15(\mathrm{stat}) \pm 0.05(\mathrm{syst})$ GeV, and for the convolution fit, $M_{\mathrm{W}} = 80.30 \pm 0.14(\mathrm{stat}) \pm 0.06(\mathrm{syst})$ GeV. As discussed in Section 5, these results are statistically consistent with those obtained using the reweighting fit.

The difference between the fitted M_{W} in the $\mathrm{W^+W^-} \to \mathrm{q\overline{q}q\overline{q}}$ and $\mathrm{W^+W^-} \to \mathrm{q\overline{q}}\ell\overline{\nu}_\ell$ channels is $\Delta M_{\mathrm{W}} \equiv (M_{\mathrm{W}}^{\mathrm{q\overline{q}q\overline{q}}} - M_{\mathrm{W}}^{\mathrm{q\overline{q}}\ell\overline{\nu}_\ell}) = 0.20 \pm 0.28 \pm 0.07$ GeV, where the uncertainties are statistical and systematic (excluding contributions from colour-reconnection/Bose-Einstein effects), respectively. A significant non-zero value for ΔM_{W} could indicate that colour-reconnection/Bose-Einstein effects are biasing the M_{W} determined from $\mathrm{W^+W^-} \to \mathrm{q\overline{q}q\overline{q}}$ events.

6.1 Combination with Previous Data

The measurements of M_{W} from direct reconstruction at $\sqrt{s} \approx 172$ GeV [5] and $\sqrt{s} \approx 183$ GeV are combined with the M_{W} measurement from the $\mathrm{W^+W^-}$ production cross-section at threshold, $\sqrt{s} \approx 161$ GeV [8]. The combination is made assuming that the mass measurements from direct

reconstruction and from the threshold cross-section are uncorrelated, apart from the uncertainty associated with the LEP beam energy, which is taken to be fully correlated. The direct reconstruction measurements are combined accounting for correlated systematics. The combined result is

$$M_{\mathrm{W}} = 80.38 \pm 0.12 \pm 0.04 \pm 0.02 \pm 0.02\,\mathrm{GeV},$$

where the uncertainties are statistical, systematic, colour-reconnection/Bose-Einstein and beam energy, respectively.

The measurements of Γ_{W} from direct reconstruction at $\sqrt{s} \approx 172$ GeV [5] and $\sqrt{s} \approx 183$ GeV are combined taking into account the correlated systematics to obtain

$$\Gamma_{\mathrm{W}} = 1.84 \pm 0.32 \pm 0.15 \pm 0.12 \pm 0.01\,\mathrm{GeV},$$

where the uncertainties are statistical, systematic, colour-reconnection/Bose-Einstein and beam energy, respectively. Monte Carlo studies reveal that the measured statistical error is correlated with the measured width. To avoid biasing the combination, the separate width measurements are weighted using the expected statistical error, determined from an ensemble of many Monte Carlo experiments assuming a W width of 2.093 GeV.

The measurements of ΔM_{W} from direct reconstruction at $\sqrt{s} \approx 172$ GeV and $\sqrt{s} \approx 183$ GeV are combined taking into account the correlated systematics to obtain

$$\Delta M_{\mathrm{W}} = 0.08 \pm 0.26 \pm 0.07\,\mathrm{GeV},$$

where the uncertainties are statistical and systematic, respectively. Note that no systematic error is included for uncertainties in the modelling of colour-reconnection/Bose-Einstein effects and that the uncertainty in the LEP beam energy does not contribute a systematic error to this quantity.

7 Summary

Using the 57 pb^{-1} of data recorded by the OPAL detector at a mean centre-of-mass energy of approximately 183 GeV, a total of 582 $\mathrm{W^+W^-} \to \mathrm{q\overline{q}q\overline{q}}$ and $\mathrm{W^+W^-} \to \mathrm{q\overline{q}}\ell\overline{\nu}_\ell$ candidate events are used in a fit constraining Γ_{W} to its Standard Model relation with M_{W} to obtain a direct measurement of the W boson mass, $M_{\mathrm{W}} = 80.39 \pm 0.13(\mathrm{stat.}) \pm 0.05(\mathrm{syst.})$ GeV, while a second fit is used to directly determine the width of the W boson, $\Gamma_{\mathrm{W}} = 1.96 \pm 0.34(\mathrm{stat.}) \pm 0.20(\mathrm{syst.})$ GeV.

The results described in this paper are combined with the previous OPAL results from data recorded at $\sqrt{s} \approx 172$ GeV and $\sqrt{s} \approx 161$ GeV. From this combined data sample the W boson mass is determined to be

$$M_{\mathrm{W}} = 80.38 \pm 0.12 \pm 0.05\,\mathrm{GeV}.$$

The result for the W boson width is combined with the previous OPAL result from data recorded at $\sqrt{s} \approx 172$ GeV to obtain

$$\Gamma_{\mathrm{W}} = 1.84 \pm 0.32 \pm 0.20\,\mathrm{GeV}.$$

The uncertainties are statistical and systematic, respectively.

Acknowledgements:

We particularly wish to thank the SL Division for the efficient operation of the LEP accelerator at all energies and for their continuing close cooperation with our experimental group. We thank our colleagues from CEA, DAPNIA/SPP, CE-Saclay for their efforts over the years on the time-of-flight and trigger systems which we continue to use. In addition to the support staff at our own institutions we are pleased to acknowledge the
Department of Energy, USA,
National Science Foundation, USA,
Particle Physics and Astronomy Research Council, UK,
Natural Sciences and Engineering Research Council, Canada,
Israel Science Foundation, administered by the Israel Academy of Science and Humanities,
Minerva Gesellschaft,
Benoziyo Center for High Energy Physics,
Japanese Ministry of Education, Science and Culture (the Monbusho) and a grant under the Monbusho International Science Research Program,
Japanese Society for the Promotion of Science (JSPS),
German Israeli Bi-national Science Foundation (GIF),
Bundesministerium für Bildung, Wissenschaft, Forschung und Technologie, Germany,
National Research Council of Canada,
Research Corporation, USA,
Hungarian Foundation for Scientific Research, OTKA T-016660, T023793 and OTKA F-023259.

References

[1] LEP Electroweak Working Group, CERN-PPE/97-154 (1997);
D. Karlen, *Experimental Status of the Standard Model*, to be published in the proceedings of the 29th International Conference on High-Energy Physics, July 1998, Vancouver, CA.

[2] W.J. Marciano and A. Sirlin, Phys. Rev. **D29** (1984) 945.

[3] See for example, G. Degrassi *et al.*, Phys. Lett. **B418** (1998) 209.

[4] UA1 Collaboration, C. Albajar *et al.*, Z. Phys. **C44** (1989) 15;
CDF Collaboration, F. Abe *et al.*, Phys. Rev. Lett. **65** (1990) 2243 Phys. Rev. **D43** (1991) 2070;
UA2 Collaboration, J. Alitti *et al.*, Phys. Lett. **B276** (1992) 354;
CDF Collaboration, F. Abe *et al.*, Phys. Rev. Lett. **75** (1995) 11 Phys. Rev. **D52** (1995) 4784;
D0 Collaboration, S. Abachi *et al.*, Phys. Rev. Lett. **77** (1996) 3309.

[5] OPAL Collaboration, K. Ackerstaff *et al.*, Eur. Phys. J. **C1** (1998) 395.

[6] DELPHI Collaboration, P. Abreu *et al.*, Eur. Phys. J. **C2** (1998) 581.

[7] L3 Collaboration, M. Acciarri *et al.*, Phys. Lett. **B413** (1997) 176;
ALEPH Collaboration, R. Barate *et al.*, Phys. Lett. **B422** (1998) 384.

[8] OPAL Collaboration, K. Ackerstaff *et al.*, Phys. Lett. **B389** (1996) 416.

[9] DELPHI Collaboration, P. Abreu *et al.*, Phys. Lett. **B397** (1997) 158;
L3 Collaboration, M. Acciarri *et al.*, Phys. Lett. **B398** (1997) 223;
ALEPH Collaboration, R. Barate *et al.*, Phys. Lett. **B401** (1997) 347.

[10] C. Caso *et al.*, Eur. Phys. J. **C3** (1998) 1.

[11] Physics at LEP2, eds. G. Altarelli, T. Sjöstrand and F. Zwirner, CERN 96-01, (1996).

[12] N. Brown and W.J. Stirling, Phys. Lett. **B252** (1990) 657;
S. Catani *et al.*, Phys. Lett. **B269** (1991) 432;
S. Bethke, Z. Kunszt, D. Soper and W.J. Stirling,Nucl. Phys. **B370** (1992) 310;
N. Brown and W.J. Stirling, Z. Phys. **C53** (1992) 629.

[13] OPAL Collaboration, M.Z. Akrawy *et al.*, Phys. Lett. **B253** (1990) 511.

[14] OPAL Collaboration, K. Ahmet *et al.*, Nucl. Instr. Meth. **A305** (1991) 275;
B.E. Anderson *et al.*, IEEE Transactions on Nuclear Science, **41** (1994) 845;
S. Anderson *et al.*, Nucl. Instr. Meth. **A403** (1998) 326.

[15] LEP Energy Working Group, A. Blondel *et al.*, *Evaluation of the LEP centre-of-mass energy above the W-pair production threshold*, CERN-SL/98-073, submitted to Eur. Phys. J. **C**.

[16] OPAL Collaboration, G. Abbiendi *et al.*, W^+W^- *production and triple gauge boson couplings at LEP energies up to 183 GeV*, CERN-EP/98-167, to be published in Eur. Phys. J. **C**.

[17] J. Allison *et al.*, Nucl. Instr. Meth. **A317** (1992) 47.

[18] M. Skrzypek *et al.*, Comput. Phys. Commun. **94** (1996) 216;
M. Skrzypek *et al.*, Phys. Lett. **B372** (1996) 289.

[19] T. Sjöstrand, Comput. Phys. Commun. **82** (1994) 74.

[20] J. Fujimoto *et al.*, Comput. Phys. Commun. **100** (1997) 128.

[21] F.A. Berends, R. Pittau and R. Kleiss, Comput. Phys. Commun. **85** (1995) 437.

[22] G. Marchesini *et al.*, Comput. Phys. Commun. **67** (1992) 465.

[23] OPAL Collaboration, G. Alexander *et al.*, Z. Phys. **C69** (1996) 543.

[24] A. Ballestrero *et al.*, J. Phys. **G24** (1998) 365.

[25] OPAL Collaboration, G. Abbiendi *et al.*, *Bose-Einstein Correlations in* $e^+e^-\to W^+W^-$ *at 172 and 183 GeV*, CERN-EP/98-174, submitted to Eur. Phys. J. **C**.

[26] DELPHI Collaboration, P. Abreu *et al.*, Phys. Lett. **B401** (1997) 181.

[27] L. Lönnblad and T. Sjöstrand, Eur. Phys. J. **C2** (1998) 165.

[28] L. Lönnblad, Z. Phys. **C70** (1996) 107.

[29] OPAL Collaboration, G. Abbiendi *et al.*, *Colour reconnection studies in* $e^+e^-\to W^+W^-$ *at* $\sqrt{s} = 183$ *GeV*, CERN-EP/98-196, submitted to Phys. Lett. **B**.

Channel	Observed	Expected	Purity
$W^+W^- \to q\bar{q}q\bar{q}$	282	278.1	86%
$W^+W^- \to q\bar{q}e\bar{\nu}_e$	119	113.0	97%
$W^+W^- \to q\bar{q}\mu\bar{\nu}_\mu$	107	114.4	99%
$W^+W^- \to q\bar{q}\tau\bar{\nu}_\tau$	74	82.6	95%
Combined	582	588.0	92%

Table 1: Numbers of events used in the W mass and width determination for each channel and all channels combined. Only events surviving the cuts described in Section 4.1 are included. The number of expected events and corresponding purities are estimated assuming the world average M_W and have relative uncertainties of approximately 3%, dominated by the uncertainty in the CC03 production cross-section.

Channel	Measured M_W	Expected error
$W^+W^- \to q\bar{q}e\bar{\nu}_e$	80.23 ± 0.24	0.31
$W^+W^- \to q\bar{q}\mu\bar{\nu}_\mu$	80.42 ± 0.27	0.30
$W^+W^- \to q\bar{q}\tau\bar{\nu}_\tau$	80.40 ± 0.40	0.45
$W^+W^- \to q\bar{q}\ell\bar{\nu}_\ell$	80.33 ± 0.17	0.19
$W^+W^- \to q\bar{q}q\bar{q}$	80.53 ± 0.23	0.20

Table 2: Results using the reweighting method for the fit constraining Γ_W to its Standard model relation with M_W from 57 pb^{-1} of data taken at $\sqrt{s} \approx 183$ GeV for each of the channels separately and for the combined $W^+W^- \to q\bar{q}\ell\bar{\nu}_\ell$ channel. The expected errors are estimated using an ensemble of Monte Carlo subsamples, each corresponding to 57 pb^{-1} of data and including background contributions. The errors are statistical only. (All quantities are in GeV.)

Channel	Breit-Wigner fit Measured M_W	Convolution fit Measured M_W
$W^+W^- \to q\bar{q}\ell\bar{\nu}_\ell$	80.27 ± 0.19	80.24 ± 0.19
$W^+W^- \to q\bar{q}q\bar{q}$	80.52 ± 0.24	80.38 ± 0.21

Table 3: Fit results using the alternative analyses and 57 pb^{-1} of data taken at $\sqrt{s} \approx 183$ GeV for the $W^+W^- \to q\bar{q}\ell\bar{\nu}_\ell$ and $W^+W^- \to q\bar{q}q\bar{q}$ channels separately. The expected statistical errors are very similar to those of the reweighting method given in Table 2. The errors are statistical only. (All quantities are in GeV.)

Systematic errors (MeV)	M_{W} $\mathrm{q\overline{q}q\overline{q}}$	$\mathrm{q\overline{q}}\ell\overline{\nu}_{\ell}$	comb.	Γ_{W}	ΔM_{W}
Beam Energy	22	22	22	5	0
Initial State Radiation	10	10	10	15	10
Hadronization	21	21	16	52	15
Four-fermion	30	28	21	52	40
Detector Effects	38	31	26	90	46
Fit Procedure	15	15	15	45	20
Background	25	10	10	79	25
MC statistics	15	15	11	40	21
Sub-total	67	58	49	154	74
Bose-Einstein Correlations	32	0	11	55	—
Colour Reconnection	49	0	16	109	—
Total systematic error	89	58	53	196	74

Table 4: Summary of the systematic uncertainties for the fit results. For the fits to determine M_{W}, Γ_{W} is constrained to its Standard Model relation. The uncertainties are given separately for fits to the $\mathrm{W^+W^-} \to \mathrm{q\overline{q}q\overline{q}}$, $\mathrm{W^+W^-} \to \mathrm{q\overline{q}}\ell\overline{\nu}_{\ell}$ and the combined samples. For Γ_{W} the uncertainties are given only for the fit to the combined sample. The quantity $\Delta M_{\mathrm{W}} \equiv \left(M_{\mathrm{W}}^{\mathrm{q\overline{q}q\overline{q}}} - M_{\mathrm{W}}^{\mathrm{q\overline{q}}\ell\overline{\nu}_{\ell}}\right)$ uses the Standard Model constrained fits to the $\mathrm{W^+W^-} \to \mathrm{q\overline{q}q\overline{q}}$ and $\mathrm{W^+W^-} \to \mathrm{q\overline{q}}\ell\overline{\nu}_{\ell}$ channels separately. Since the primary interest in the quantity ΔM_{W} is as a test of possible colour-reconnection/Bose-Einstein effects in the $\mathrm{W^+W^-} \to \mathrm{q\overline{q}q\overline{q}}$ channel, no systematic error is assigned for uncertainties associated with the modelling of these effects. The inter-channel correlations are taken into account for the combined M_{W} and Γ_{W} fits and for the ΔM_{W} determination.

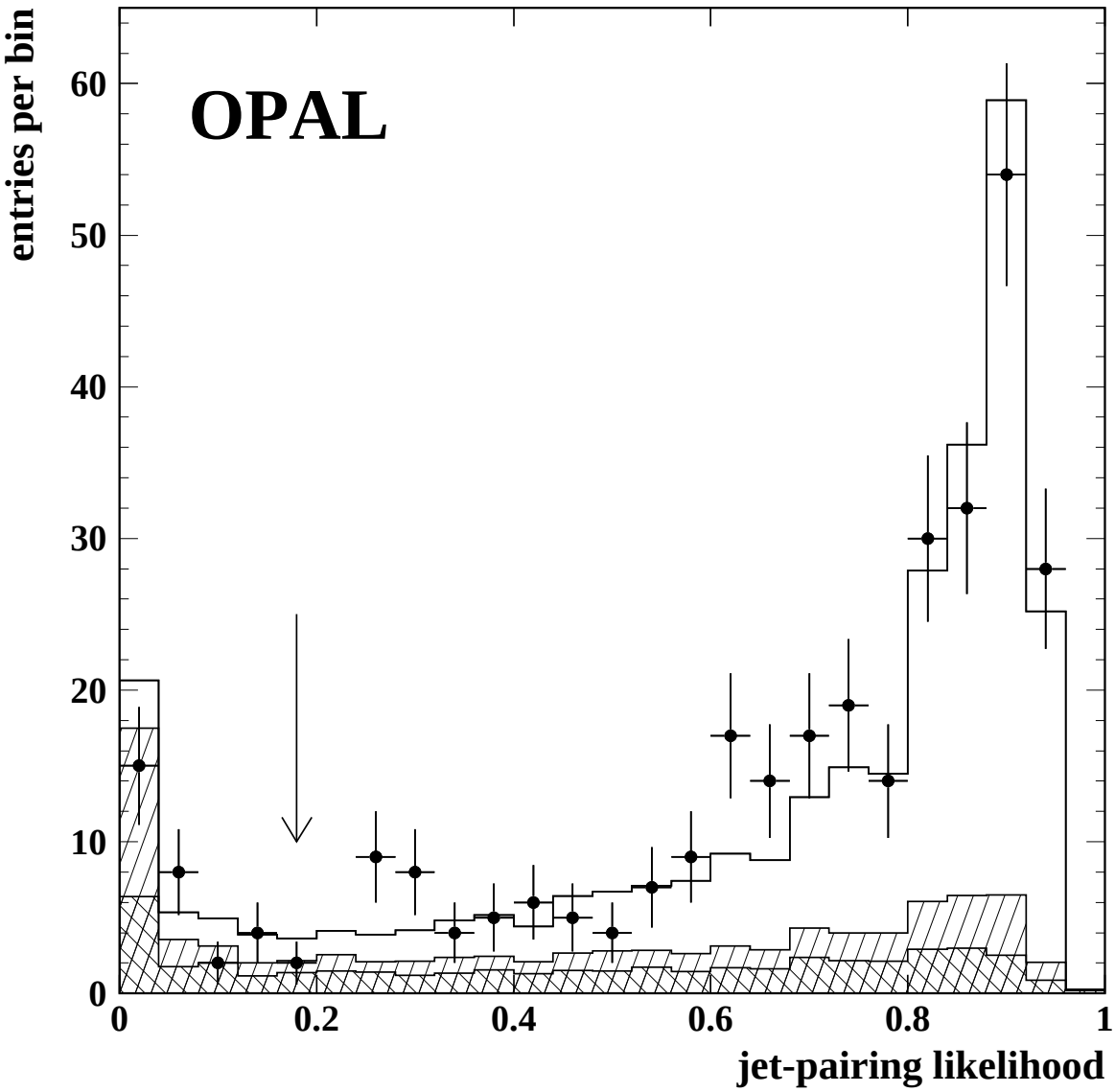

Figure 1: The jet-pairing likelihood distribution for selected $W^+W^- \to q\overline{q}q\overline{q}$ events. For each event, only the likelihood output for the combination yielding the maximum likelihood is plotted. Events to the right of the arrow are retained for the mass analysis. The points correspond to the OPAL data and the open histogram to the Monte Carlo prediction. The contribution from the non-WW background is shown as the cross-hatched histogram and the addition of the combinatorial background is indicated by the singly-hatched histogram.

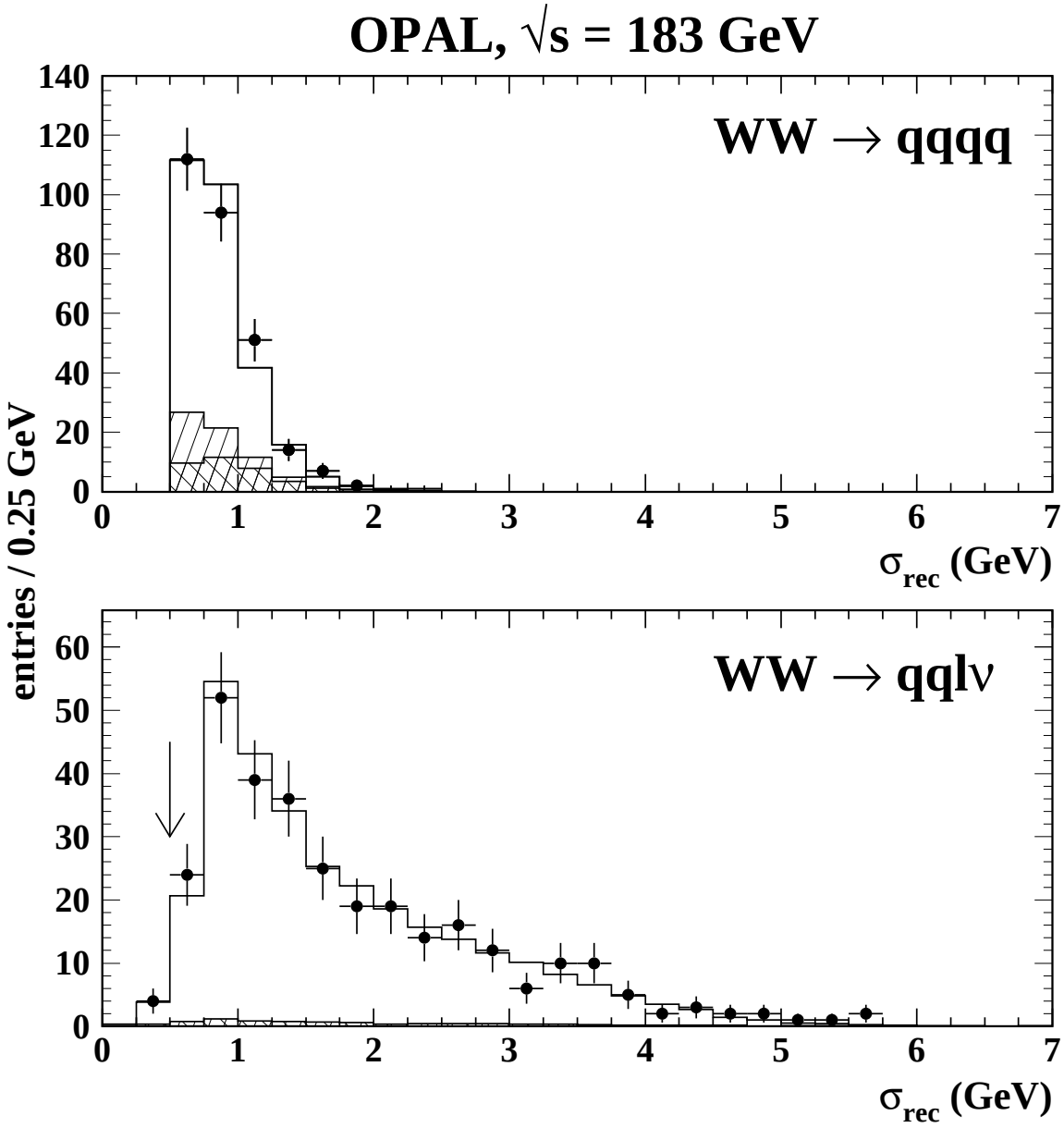

Figure 2: The distribution of the error on the reconstructed invariant mass, $\sigma_{\rm rec}$, for $\mathrm{W^+W^-} \to \mathrm{q\overline{q}q\overline{q}}$ events surviving the jet-pairing likelihood cut and used in the mass analysis (top), and for all selected $\mathrm{W^+W^-} \to \mathrm{q\overline{q}}\ell\overline{\nu}_\ell$ events (bottom). The $\mathrm{W^+W^-} \to \mathrm{q\overline{q}}\ell\overline{\nu}_\ell$ events to the right of the arrow are retained for the mass analysis. This error is used to divide the $\mathrm{W^+W^-} \to \mathrm{q\overline{q}}\ell\overline{\nu}_\ell$ events into four subsamples: $0.5 < \sigma_{\rm rec} < 1.5$ GeV, $1.5 < \sigma_{\rm rec} < 2.5$ GeV, $2.5 < \sigma_{\rm rec} < 3.5$ GeV, $\sigma_{\rm rec} > 3.5$ GeV, which are chosen to minimize the expected statistical error on $M_{\rm W}$. The points correspond to the OPAL data and the open histogram to the Monte Carlo prediction. The background contribution is indicated by the cross-hatched histogram. In the $\mathrm{W^+W^-} \to \mathrm{q\overline{q}q\overline{q}}$ channel, the addition of the combinatorial background is indicated by the singly-hatched histogram.

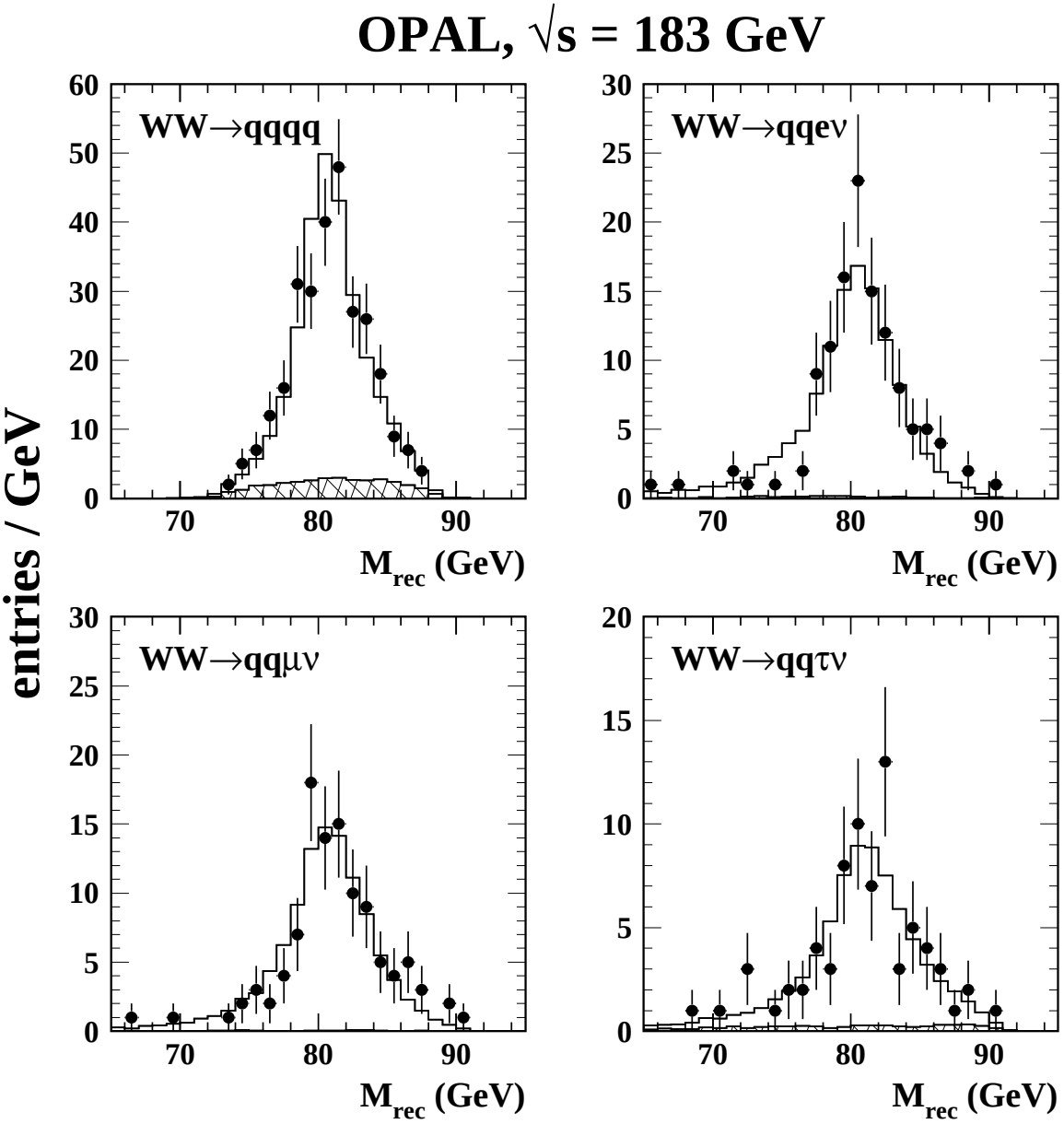

Figure 3: The reconstructed invariant mass distribution for the $W^+W^- \to q\overline{q}q\overline{q}$, $W^+W^- \to q\overline{q}e\overline{\nu}_e$, $W^+W^- \to q\overline{q}\mu\overline{\nu}_\mu$ and $W^+W^- \to q\overline{q}\tau\overline{\nu}_\tau$ samples. The points correspond to the OPAL data and the open histogram to the reweighted Monte Carlo spectrum corresponding to the fitted mass. The background contribution is indicated by the cross-hatched histogram.

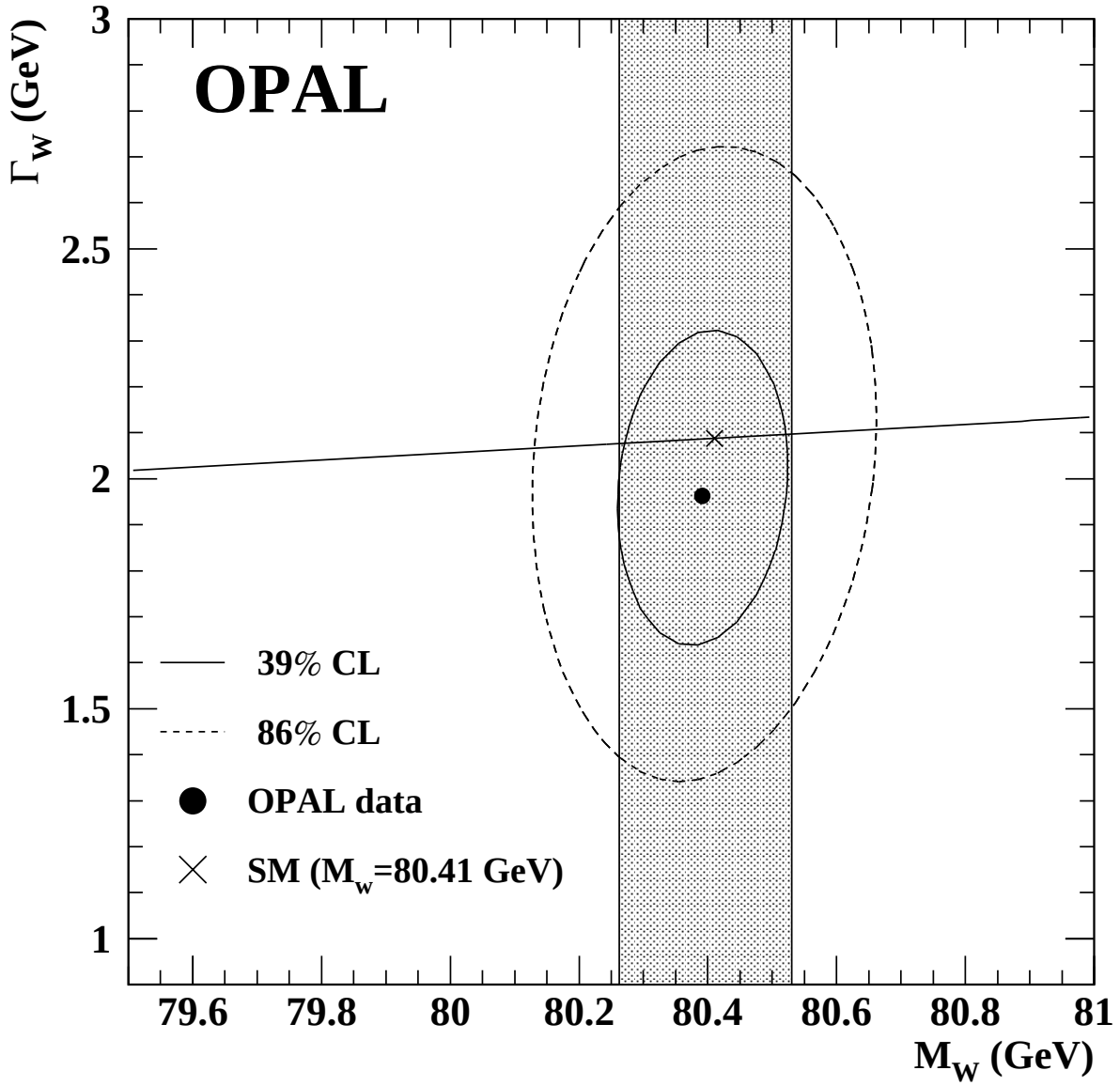

Figure 4: The 39% and 86% contour levels of the two-parameter fit using the reweighting method. The projections of these contours onto the axes give the one and two standard deviation statistical uncertainties. The one standard deviation region, including only the statistical error, of the fit to M_{W} only is given by the shaded band. This fit is constrained to the solid line, which gives the dependence of the width on the mass according to the Standard Model. The Standard Model prediction for Γ_{W}, assuming the world average M_{W}, is shown as an "X".